

## RESEARCH ARTICLE

10.1002/2014JC010502

## Large icebergs characteristics from altimeter waveforms analysis

J. Tournadre<sup>1</sup>, N. Bouhier<sup>1</sup>, F. Girard-Ardhuin<sup>1</sup>, and F. Rémy<sup>2</sup><sup>1</sup>Laboratoire d'Océanographie Spatiale, IFREMER, Plouzané, France, <sup>2</sup>LEGOS (CNRS-CNES-IRD-UPS), Toulouse, France

## Key Points:

- New technique to measure the freeboard of large icebergs
- Analysis of the volume of ice and its variability for the 2002–2012 period
- Estimation of the melt rate and breaking of large iceberg

## Supporting Information:

- Supporting Information S1
- Figures S1–S3
- Table S1

## Correspondence to:

J. Tournadre,  
jean.tournadre@ifremer.fr

## Citation:

Tournadre, J., N. Bouhier, F. Girard-Ardhuin, and F. Rémy (2015), Large icebergs characteristics from altimeter waveforms analysis, *J. Geophys. Res. Oceans*, 120, 1954–1974, doi:10.1002/2014JC010502.

Received 10 OCT 2014

Accepted 11 FEB 2015

Accepted article online 18 FEB 2015

Published online 26 MAR 2015

**Abstract** Large uncertainties exist on the volume of ice transported by the Southern Ocean large icebergs, a key parameter for climate studies, because of the paucity of information, especially on iceberg thickness. Using icebergs tracks from the National Ice Center (NIC) and Brigham Young University (BYU) databases to select altimeter data over icebergs and a method of analysis of altimeter waveforms, a database of 5366 icebergs freeboard elevation, length, and backscatter covering the 2002–2012 period has been created. The database is analyzed in terms of distributions of freeboard, length, and backscatter showing differences as a function of the iceberg's quadrant of origin. The database allows to analyze the temporal evolution of icebergs and to estimate a melt rate of 35–39 m·yr<sup>-1</sup> (neglecting the firn compaction). The total daily volume of ice, estimated by combining the NIC and altimeter sizes and the altimeter freeboards, regularly decreases from 2.2 10<sup>4</sup>km<sup>3</sup> in 2002 to 0.9 10<sup>4</sup>km<sup>3</sup> in 2012. During this decade, the total loss of ice (~1800 km<sup>3</sup>·yr<sup>-1</sup>) is twice as large as than the input (~960 km<sup>3</sup>·yr<sup>-1</sup>) showing that the system is out of equilibrium after a very large input of ice between 1997 and 2002. Breaking into small icebergs represents 80% (~1500 km<sup>3</sup>·yr<sup>-1</sup>) of the total ice loss while basal melting is only 18% (~320 km<sup>3</sup>·yr<sup>-1</sup>). Small icebergs are thus the major vector of freshwater input in the Southern Ocean.

## 1. Introduction

Interest in icebergs has been growing in the recent years [see e.g., *Smith*, 2011 review] because they account for a large fraction of the annual mass loss of the Antarctica Ice Sheet [*Benn et al.*, 2007; *Depoorter et al.*, 2013; *Rignot et al.*, 2013]; they may also account for a significant part of the freshwater flux in the Southern Ocean [*Silva et al.*, 2006; *Martin and Adcroft*, 2010; *Gladstone et al.*, 2001] and can thus impact the deep water formation [*Silva et al.*, 2006; *Jongma et al.*, 2009], and because they have been shown to transport nutrient (in particular labile iron) that could have a significant impact on ocean primary productivity [*Schodlok et al.*, 2006; *Raiswell et al.*, 2008; *Lancelot et al.*, 2009; *Schwarz and Schodlok*, 2009]. Large icebergs generated by the collapse or disintegration of the Antarctica ice shelves or by calving from glaciers are thought to transport, on average, an amount of ice comparable to the amount transported by the whole population of smaller icebergs [*Jacobs et al.*, 1992]. The dimensions of the large southern icebergs are regularly estimated using visible or SAR images by the National Ice Center (NIC), but very few direct measurements of iceberg freeboard and thus of iceberg volume exist. In general, the volume of ice is estimated using proxies of the iceberg thickness such as the thickness of ice shelves and emissary glaciers [*Gladstone et al.*, 2001]. Thus, large uncertainties still exist on the total ice volume of icebergs as well as on the intensity of icebergs melting [*Jansen et al.*, 2007].

Elevation profiles measured by the Geoscience Laser Altimeter System (GLAS) instrument aboard the Ice, Cloud, and land Elevation (ICESat) satellite have been used to study a few icebergs [*Scambos et al.*, 2005; *Jansen et al.*, 2007]. But, up to now, no large database of freeboard elevation measurements exists.

Since the launch of Seasat, the potential of altimeter data to estimate iceberg's freeboard has been explored [*McIntyre and Cudlip*, 1987] and some examples of freeboard profiles have been published. However, the first generation of altimeters (Seasat, Geosat, Topex/Poseidon) used on-board trackers that frequently loose the surface during rapid transitions of elevation resulting in a several second long loss of data, which greatly hampered the possibility of iceberg freeboard measurement. Since the launch of Jason-1 and Envisat in 2002, the technological progress in altimetry allows to better cope with the rapid elevations changes occurring over a large iceberg or a coast [*Gommenginger et al.*, 2011] opening a new opportunity to measuring

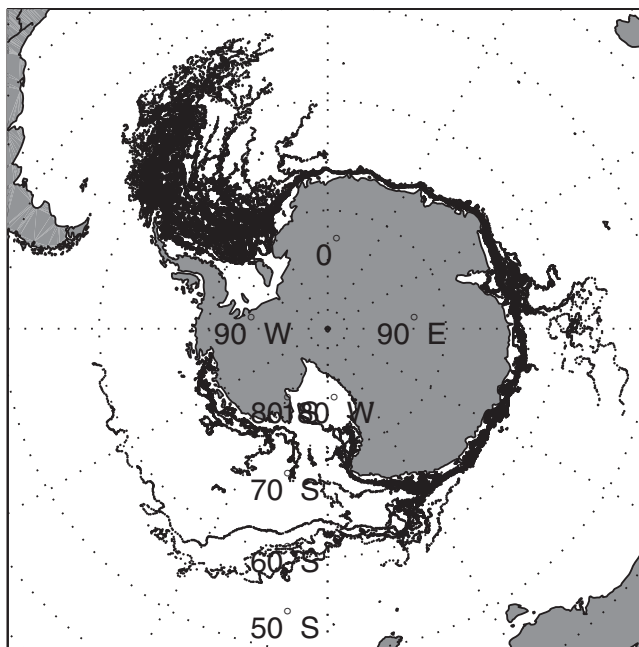


Figure 1. Icebergs locations from the BYU database for 2002–2012 period.

icebergs freeboards on a quasiroutine basis. To create a database of freeboards, it is necessary first to detect icebergs and then to estimate their characteristics from altimeter data analysis. The tracks of large icebergs, produced by NIC and by the Brigham Young University (BYU) Center for Remote Sensing can be used to detect icebergs in altimeter data by simple collocation in time and space. The collocated altimeter data can then be analyzed in terms of iceberg characteristics.

Section 2 describes the icebergs databases and the altimeter data used in the study. The method of analysis of altimeter data over iceberg and the validation of altimeter freeboard profiles are presented in section 3. The altimeter iceberg database is analyzed in

terms of freeboard, length, and backscatter distributions in section 4. The evolution of icebergs, the estimate of basal melt rate, the volume of ice, and the different terms (input by calving, melting, and breaking) contributing to its evolution are presented in section 5 as well as the surface backscatter of iceberg.

## 2. Data

### 2.1. The NIC and BYU Database

The NIC Southern Hemisphere Iceberg database, freely available from their Web site (<http://www.natice.noaa.gov>), contains the position and size (length and width) estimated by analysis of visible or SAR images of icebergs larger than 10 nautical miles (19 km) along at least one axis. It is updated weekly. Every iceberg is tracked, and when imagery is available, information is updated and posted. The NIC is the only organization that names and tracks all these large Antarctic icebergs. It assigns each iceberg a name composed of a letter indicating its point of origin and a running number. The letters used are as follows: A—longitude  $0^{\circ}$ – $90^{\circ}$  W (Bellingshausen Sea, Weddell Sea); B—longitude  $90^{\circ}$ W– $180^{\circ}$  (Amundsen Sea, Eastern Ross Sea); C—longitude  $90^{\circ}$ E– $180^{\circ}$  (Western Ross Sea, Wilkes Land); D—longitude  $0^{\circ}$ – $90^{\circ}$  E (Amery Ice Shelf, Eastern Weddell Sea). Chris Readinger (personal communication) provided us with a copy of the iceberg tables from 2002 to 2010 (with few data in 2009) and from September 2013 to April 2014.

The BYU Center for Remote Sensing maintains an Antarctic Iceberg Tracking Database (<http://www.scp.byu.edu/data/iceberg/database1.html>) for icebergs larger than 6 km in length [Stuart and Long, 2011]. Using six different satellite scatterometer instruments, they produced an iceberg tracking database that includes icebergs identified in enhanced resolution scatterometer backscatter images during July–September 1978 (from Seasat), July 1996 to June 1997 (from NSCAT), and 1992–2001 (from ERS-1/2). The initial position for each iceberg is located based on a position reported by NIC or by the sighting of a moving iceberg in a time series of scatterometer images. The iceberg name is the NIC one except for those detected in scatterometer data only that are named UK (for “unknown”). Figure 1 presents all the iceberg locations between 1 January 2002 and 31 December 2012 used in this study. The BYU database contains all NIC icebergs plus additional icebergs detected in the scatterometer images. For the 2002–2012 period considered in this study, among the 309 icebergs, 113 icebergs are common to NIC and BYU databases, and 196 are “unknown.” Supporting information Figures S1–S3 present of all the icebergs detected during the period.

## 2.2. The Altimeter Waveforms Data

An altimeter is a nadir looking radar that emits short pulses that are backscattered by the surface. The altimeter measures the backscattered power as a function of time to construct the echo waveform from which the geophysical parameters are estimated [Chelton *et al.*, 2001]. Surface height is the difference between the satellite's position on orbit with respect to an arbitrary reference surface (the Earth's center or a reference ellipsoid) and the satellite-to-surface range (calculated by measuring the time taken by the signal to make the round trip). Besides surface height, by looking at the return signal's amplitude and waveform, we can also measure wave height and wind speed over the oceans, and more generally, backscatter coefficient and surface roughness for most surfaces off which the signal is reflected [Brown, 1977; Chelton *et al.*, 2001].

The major stages in the acquisition and tracking of the waveforms are as follows. In order to keep the waveforms well centered in range and power in the analysis window and to better adjust these parameters for the echoes to come, the on-board altimeter calculator processes a few radar echoes that the receiver just recorded. It anticipates the settings for the forthcoming echo from a treatment of a number of those past echoes. When this fast on-board tracking function is not able to adjust these parameters under critical conditions, such as a transition from sea to iceberg, the altimeter loses lock. After a tracker loss, the altimeter switches to an acquisition phase, searching for the signal, locking onto it, and stabilizing the tracking loops. This acquisition sequence lasts from some tenths of second to 3 s (for Envisat) and there is no data during this, until the tracking is properly reinitialized.

Three altimeters have been used in this study, i.e., Envisat (15 April 2002 to 30 March 2012), Jason-1 (1 January 2002 to 31 December 2012), Jason-2 (26 August 2008 to 31 December 2012). Detailed descriptions of the sensors and missions are given in Resti *et al.* [1999], Ménard and Fu [2001], and Lambin *et al.* [2010], respectively, and Table 1 summarizes their main technical and orbital characteristics. Others altimeters such as AltiKa or Cryosat could also be used in the future to enrich the database. The Sensor Geophysical Data Records containing the 20 Hz echo waveforms necessary to the study were provided by AVISO for Jason-1 and Jason-2 and by the European Space Agency for Envisat.

## 3. Method

### 3.1. Echo Waveforms Simulation Over a Large Iceberg and Detection Method

Using the analytical waveform model of Tournadre *et al.* [2011], Jason-2 waveforms over a rectangular iceberg of  $30 \times 20 \text{ km}^2$  and 28 m freeboard have been computed. The sea backscatter was set to 10 dB and the ice backscatter to 18 dB, a random noise of 1 dB was added to both backscatters. Two simulations were conducted. First, the waveforms were computed assuming that the altimeter tracker perfectly follows the surface (see Figure 2a), i.e., that the surface always corresponds to the altimeter nominal track point (0). The waveforms are computed only within the altimeter nominal analysis window (bins  $-32$  to  $72$  for Jason-2, each bin has a length equal to the altimeter pulse length or 0.47 m). As the altimeter approaches the iceberg, backscatter from its surface appears in the plateau region part of the waveform, i.e., at far range, and grows in intensity while moving toward and pass the nominal track point until the tracker jumps to the iceberg surface. A symmetrical behavior occurs when the altimeter leaves the iceberg.

The second simulation assumes that the tracker is locked on the zero altitude (mean sea surface) and that the analysis window is large enough to capture the echo from the iceberg (here from bin  $-70$  to  $104$ ). This simulation enables computing the complete echo waveforms from the iceberg (Figure 2b). For comparison, the waveforms of the first simulation are remapped using the tracker position, i.e., each waveform is simply translated of the number of telemetry bins corresponding to the tracker position (Figure 2c). This remapping also allows a better and direct visualization of the iceberg signature. The comparison of the simulations

**Table 1.** Main Characteristics of the Radar Altimeters Used to Build the Database

Altimeter	Time Period	Altitude (km)	Inclination	Frequency (GHz)	Numbers of Bins	Track point	bin Width (ns)	Tracker
Jason1	2002–2012	1334	66°	Ku-13.6	104	32.5	3.125	Split Gate Tracker
Envisat	2002–2012	784	98°	Ku-13.575	128	43	3.125	Model-free tracker
Jason2	2008-	1334	66°	Ku-13.5	104	32.5	3.125	Median/DEM

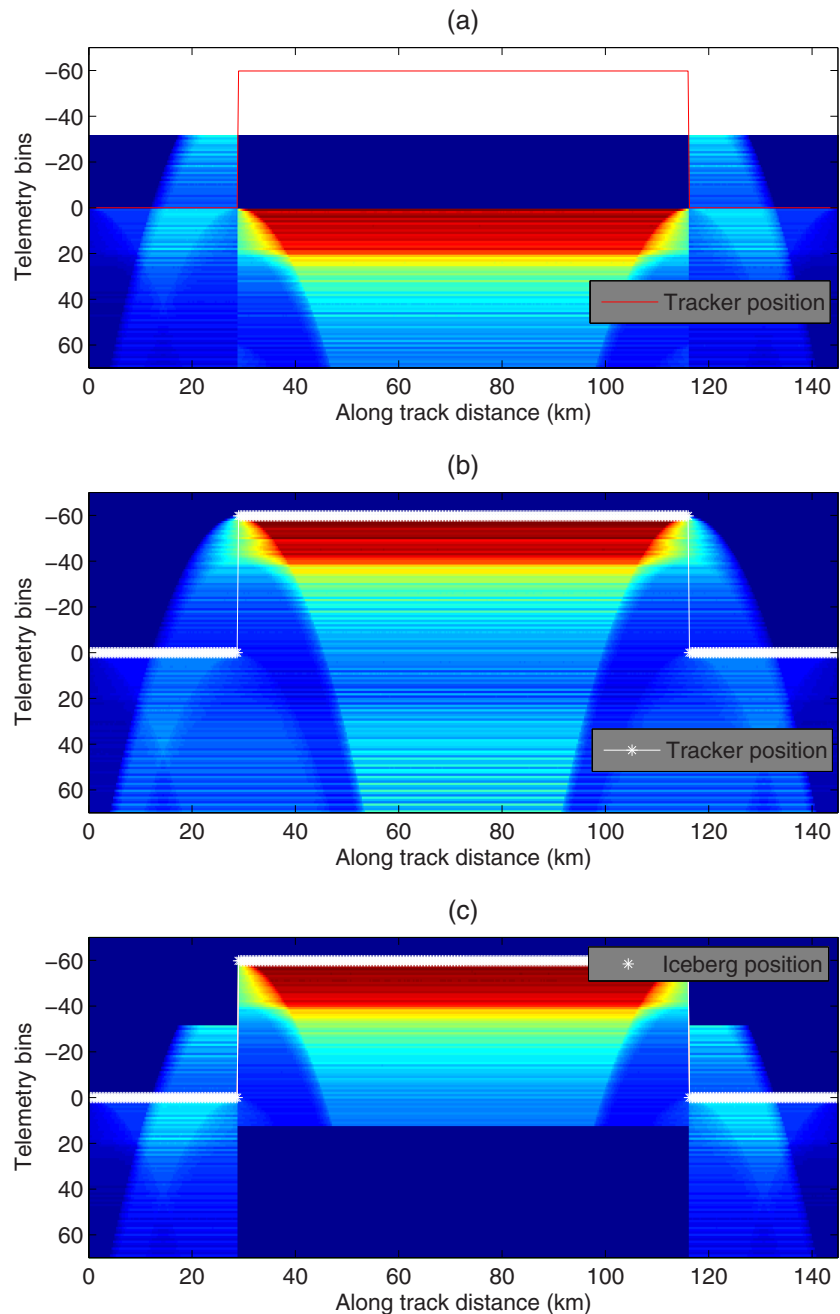


**Figure 2.** Simulated Jason-2 altimeter waveforms over a  $30 \times 20 \text{ km}^2$  and 28 m freeboard rectangular iceberg, for a tracker following the surface and a limited analysis window (a), and for a tracker locked at 0 (sea surface) and an extended analysis window (b). Waveforms of Figure 2a remapped using the tracker position (c). The red line in Figure 2a is the tracker position in telemetry bins and the white lines in Figures 2b and 2c represent the tracker position and the detected surface using iceT retracking, respectively.

shows that the only notable differences are near the iceberg edges where the nominal limited analysis window results in the loss of a small part of the waveforms.

When the tracker perfectly follows the surface, its position is a direct measurement of the freeboard profile. However, the analysis of real data shows that it is rarely the case and that it is in general necessary to retrack the waveform by fitting an analytical model to obtain a precise height estimate. Over ice the best retracking algorithm is the ICE-2 retracker [Legrésy, 1995], which is used in parallel to the classical ocean Brown model to process all the Jason-2 and Envisat data but not yet the Jason-1 data. As the precision of elevation required to study icebergs does not need to reach the centimeter level as for ocean studies, a simplified

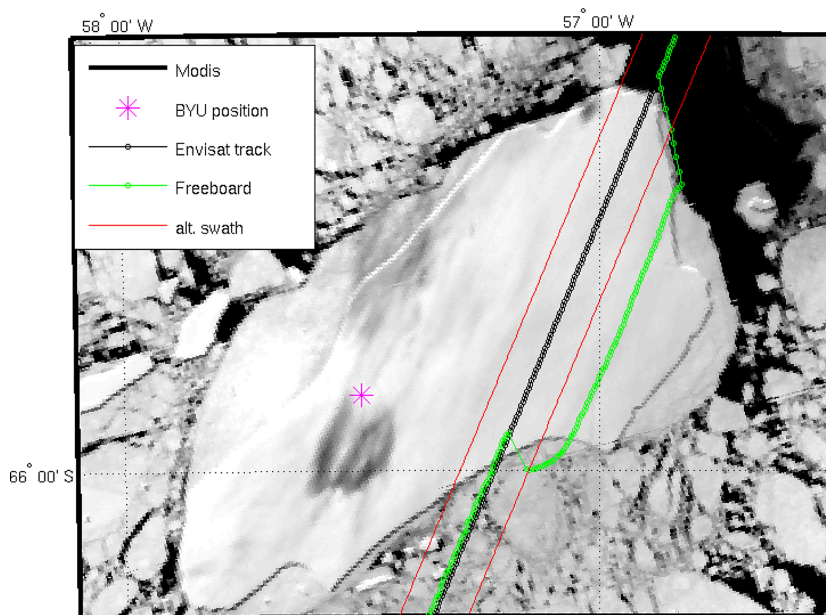


**Figure 3.** MODIS image of iceberg A43A on 2 October 2003 13:20 UT and ENVISAT RA2 ground track (fine black line) and freeboard profile (green line) on 1 October 2003 12:35 UT. The two red lines indicate the width of the altimeter swath and the magenta star the location of the iceberg in the BYU database.

algorithm based on ICE2 (hereafter called iceT) has been developed to detect the iceberg surface. It is based on the detection for each waveform of the first occurrence (bin) of a power gradient larger than a given threshold. By design, the precision of iceT cannot be better than 1 telemetry bin, i.e., 0.47 m. The elevation estimated by this algorithm for the first simulation and presented in Figure 2c gives very good results at one bin precision.

### 3.2. Example of Waveforms Over an Iceberg

Figures 3 and 4 present one example of altimeter data over iceberg A43a. On 2 October 2003 Envisat flew over iceberg A43a (Cycle 20 pass 476 descending pass) in the Weddell Sea (Figure 3). The waveforms corresponding to this pass, and the remapped waveforms using the tracker position are presented in Figures 4a and 4b respectively. As the altimeter approaches the iceberg from the north near 5.65°S, the tracker starts to move up mitigating the sea and iceberg surface elevations. As the tracker is not locked on the iceberg surface, the strong echo from the iceberg starts to appear in the first gate of the waveforms then moves toward the nominal track point (0) while the echo from the sea surface moves away from zero. Moving further, the tracker “overshoots” and continues to move up for a few tenth of seconds before locking on the surface. A symmetrical behavior occurs when the altimeter leaves the iceberg. The tracker starts to mitigate the iceberg and sea surface, and then slightly overshoots downward before relocking on the sea surface. In this particular case, it is worth noting that the altimeter ground track is almost perpendicular to the iceberg edge to the north, which gives a sharp elevation transition, while the track intersects the southern edge at a slanted angle resulting in a much longer transition during which the altimeter footprint contains both ocean and iceberg.

The comparison of the ocean, ICE2, and iceT retracker presented in Figure 4c shows a very good agreement over the iceberg. The difference is about 1 telemetry bin (0.47 m) over the core of the iceberg. The notable differences occur near the edges where ICE2, because of its design, detects the strong sea ice echo instead of the weaker iceberg’s one. In this particular case, the classical ocean retracker gives similar results as the iceT one. The MODIS brightness profile along the Envisat ground track shows that the length of iceberg estimated from the altimeter elevation profile is equivalent to the one from MODIS data. The 1–2 km translation between the profiles is within the uncertainties of localization of the MODIS image and the altimeter data.

The backscatter profile (Figure 4d) also clearly shows the sea ice/water—iceberg transition with a variation of more than 5 dB. The shaded zone in the figure corresponds to the section of the track where only the iceberg contributes to backscatter.

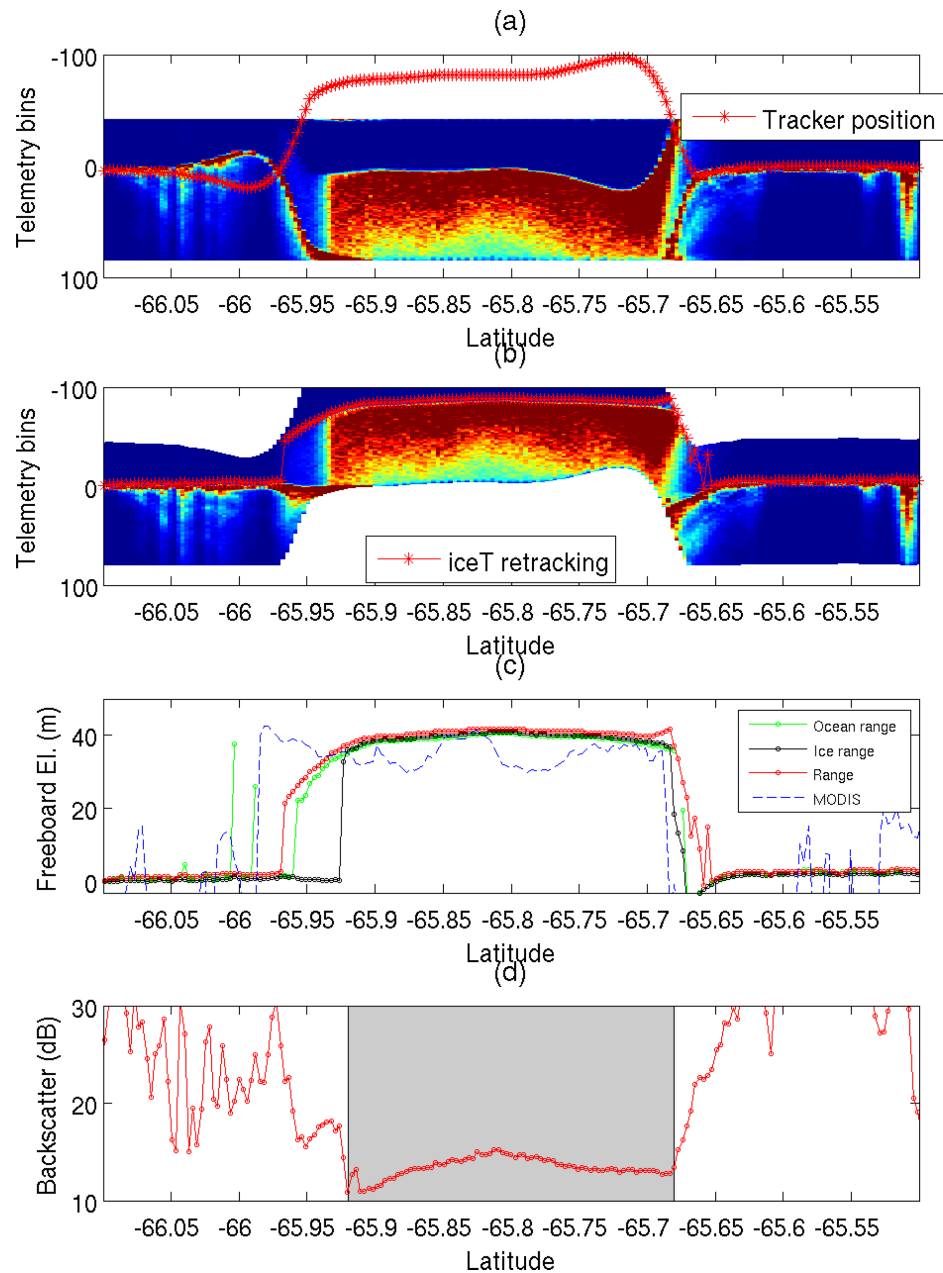


**Figure 4.** Altimeter waveform for the Envisat pass of Figure 3. The red line indicates the tracker position (a). Retracked waveforms using the tracker position, the red stars represent the iceT freeboard positions (b). Elevations from the MLE3 retracker (green line), the ICE2 retracker (black line), and iceT one (red line), and MODIS brightness (blue line)(c). Measured backscatter Figure 4d. The shaded area represents the zone over which only the iceberg surface is seen by the altimeter.

For each detected iceberg, the waveforms are analyzed and the following characteristics are estimated: the iceberg freeboard profile ( $h$ ), the mean freeboard ( $\bar{h}$ ), the maximum freeboard ( $h_m$ ), the backscatter profile ( $\sigma_0$ ), the mean backscatter (over the core of the iceberg, i.e., the shaded area of Figure 4d) ( $\bar{\sigma}_0$ ), the maximum backscatter ( $\sigma_{0m}$ ), and the length of the iceberg ( $L$ ) (for freeboards larger than 0). The backscatters from the different altimeters have been intercalibrated using the calibration coefficients of *Queffelec* [2013]. For some particular cases, e.g., when two icebergs are very close to each other, freeboard profiles can be manually analyzed and corrected.

### 3.3. Comparison With Icesat Profiles

A direct comparison of altimeter freeboard with other sources of data is difficult, first, because of the scarcity of available data and, second, because a precise collocation in time and space of measurements from

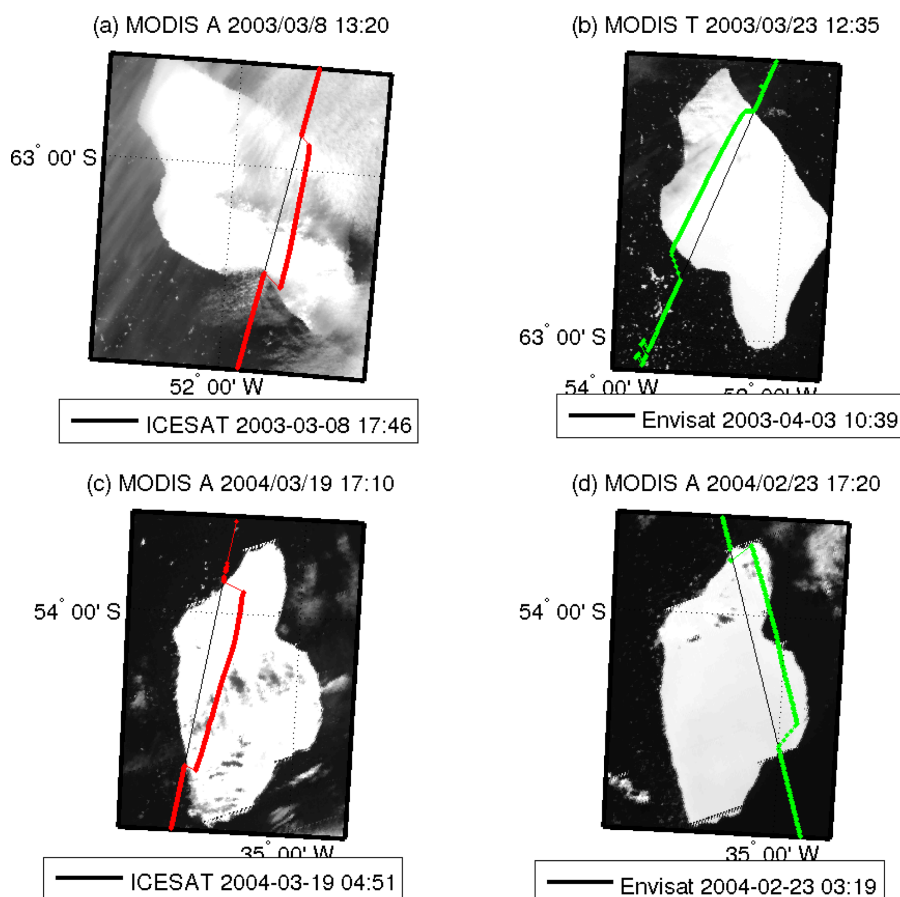


Figure 5. MODIS images and ICESat (a and c) or Envisat (b and d) profiles in March 2003 and 2004 over A38b iceberg.

different sources is hampered by the drift and rotation of icebergs. However, it is important at least for a few cases to compare the altimeter estimates with the precise freeboard measurements provided by the GLAS instrument on ICESat. Iceberg A38b that has been studied in detail by Scambos *et al.* [2005] using GLAS/ICESat profiles and by Jansen *et al.* [2007] using models and ICESat data constitutes a very good test case for the validation of altimeter data. Figure 5 presents MODIS images of iceberg A38b as well as collocated ICESat and Envisat ground tracks. The four tracks sample different parts of the iceberg of different freeboards. In their 2007 study, Jansen *et al.* [2007] presented maps of A38b freeboard based on an initial shape estimated from Ice shelf elevation data and a melting model calibrated using the ICESat profiles of Figure 5. The maps for March 2003 and 2004 are presented in Figure 6 as well as the ICESat and Envisat ground tracks. These maps are used to intercompare the Envisat and ICESat freeboard profiles of Figure 7. The data from Jansen *et al.* [2007] are interpolated along the Envisat profiles and are presented in the figure (dashed lines). For March 2003, the difference between the Envisat and model profiles is less than 1 m and in March 2004 it is of the order of 1.5 m. As the model was calibrated using the GLAS data, the model data interpolated along the GLAS profile are not presented. This comparison shows the very good agreement between Envisat, the model, and GLAS.

#### 4. The Database of Altimeter Measurements Over Large Icebergs

##### 4.1. Global Analysis

The collocation of the NIC/BYU and altimeter databases gives more than 7000 hits among which 5366 were exploitable and processed. All the 113 (40 A quadrant, 38 B, 29 C, 8 D) NIC icebergs of the 2002–2012 period but 3 (from quadrant A) were sampled at least once by an altimeter, and 95 of the 196 smaller “UK” BYU icebergs were also sampled. The mean number of samplings for an iceberg is 43 (53 for the NIC ones) and

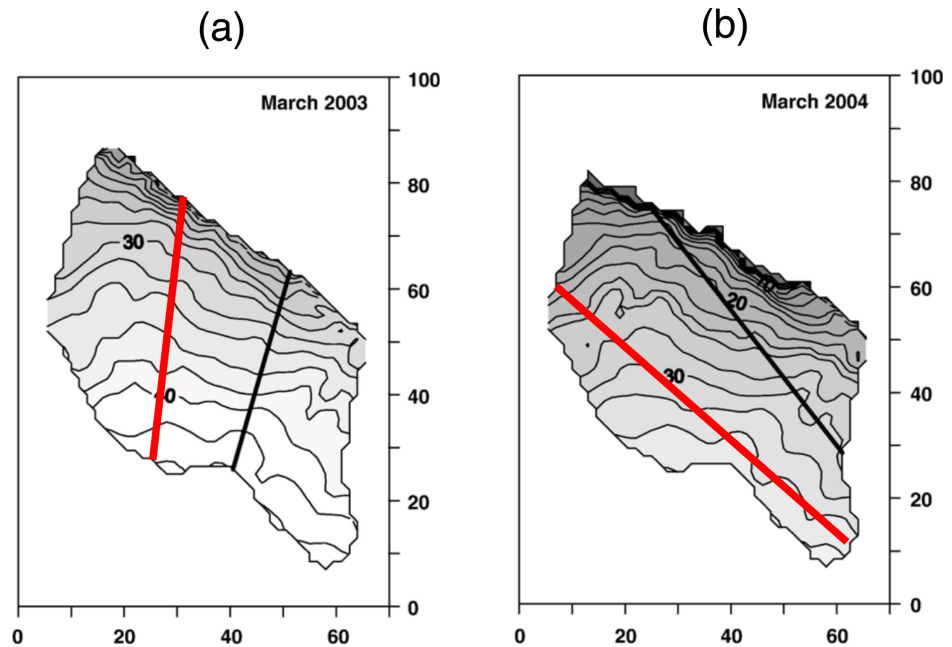


**Figure 6.** A38b freeboard maps for March 2003 (a) and March 2004 (b) from *Jansen et al.* [2007]. The black lines represent the ICESat profiles on 3 March 2003 (a) and 19 March 2004 (b) while the red lines represent the Envisat ones on 22 March 2003 (a) and 22 February 2004 (b).

varies from 1 to 354. The mean time between two samplings is 43 days (32 for NIC) with a minimum of 5.5 days and a maximum of 680 days. The details of the sampling of each iceberg are provided in supporting information Table S1. The mean standard deviation of elevation for the freeboard profiles is  $3 \pm 0.9$  m.

The histograms of freeboard, backscatter, length, and year of measurement are presented in Figure 8 while the mean length and freeboard are given in Table 2. The freeboard distribution is clearly multimodal with maximums at 35, 42, and 55 m. The backscatter distribution is almost Gaussian with a mean of 13.7 dB and a standard deviation of 3.2 dB. The iceberg length follows well a lognormal distribution of 39.5 km mean. This value is between the mean 48 km length and the mean 21 km width of the NIC icebergs. It is of the order of the mean square root of the NIC iceberg's surface (31 km). The number of measurements per year is quite constant.

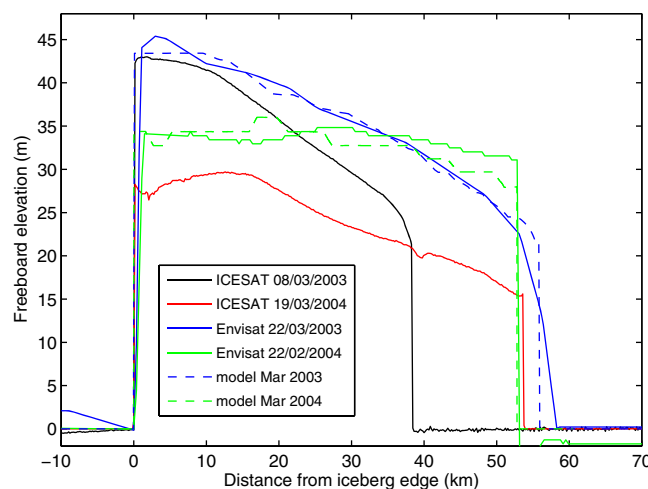


**Figure 7.** Comparison of ICESat (black and red solid lines) and Envisat (blue and green solid lines) freeboard elevation profiles of A38b. The profiles modeled by *Jansen et al.* [2007] for March 2003 and 2004 are presented as green and blue dashed lines.

The data have been sorted according to the iceberg quadrant of origin, (first letter of the iceberg name). The number of icebergs, the number of measurements, the mean length, and freeboard for each quadrant are also given in Table 2. The histograms of freeboard, backscatter, and length computed as a function of origin presented in Figure 9 show that the iceberg populations differ sensibly for the different sectors. Indeed, if the backscatter distributions, which reflect the electromagnetic behavior of ice, are quite similar, the distributions of freeboard and length differ notably. Quadrant B, for which the largest number of measurements is available, has an almost Gaussian freeboard distribution and presents the largest

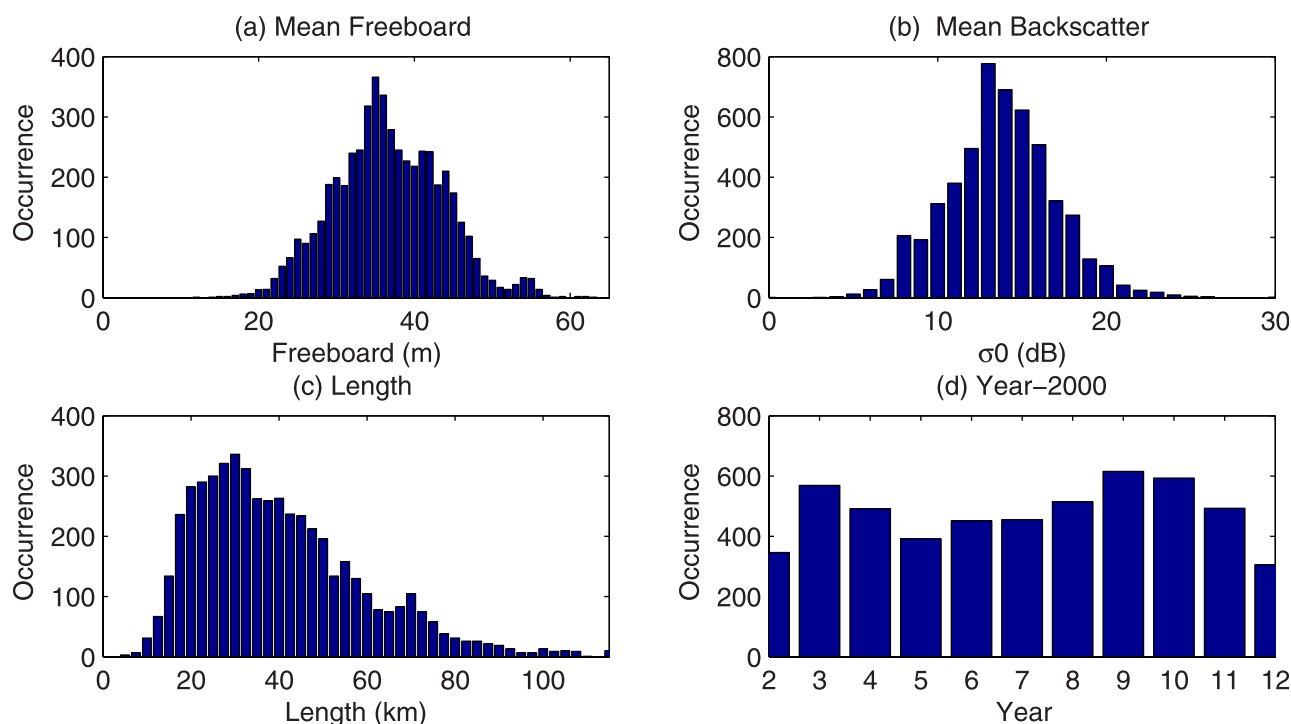


Figure 8. Distributions of (a) mean freeboard, (b) mean backscatter, (c) length, and (d) year of detection.

mean freeboard (39.5 m) while the length distribution follows a lognormal distribution of 40 km mean. Quadrant A presents bimodal freeboard and length distributions with maximums at 36 m and 55 m and 40 km and 70 km, respectively. Quadrant C has the lowest mean freeboard and length (33 m and 36 km, respectively) of all sectors. In sector D, few measurements (241) are available and they correspond mainly to one single iceberg (D15). The mean freeboard and length are 36 m and 72 km, respectively, but the data set representativeness is quite low. The last group of icebergs that does not correspond to a geographic sector but to the “unknown” icebergs detected by BYU using scatterometer data are characterized by the lowest mean length (21 km) and freeboard (32 m).

Figure 10 presents the scatter plots of all freeboard, backscatter, and length measurements as well as their mean values over a regular 150 × 150 km<sup>2</sup> regular polar grid. The largest freeboards are observed in the Amundsen Sea with a mean value of 40 m, along the East Antarctica coast with local maximums near the Amery ice shelf and the Mertz Glacier and in the eastern Weddell Sea. The icebergs’ melting during their travel to the north is clearly visible in the general decreasing trend of freeboard towards the north especially in the South Atlantic and Pacific Oceans. The melting also partially reflects in an increase of surface backscatter. It is, however, more difficult to define a trend as the freeboard one. The interpretation of the variation of length is more difficult as altimeters might sample only a small portion of a large iceberg. However, the mean length field clearly shows that the largest icebergs travel within the Antarctic coastal current and in the Weddell Sea along the Antarctic Peninsula. The large values observed in the South Pacific

Table 2. Statistical Analysis of the NIC and Altimeter Iceberg Databases

Database	National Ice Center				Altimeter							
	A-B-C-D	A	B	C	D	A-B-C-D-Unk	A-B-C-D	A	B	C	D	Unk
Number of icebergs	115	40	38	29	8	207	112	37	38	29	8	95
Number of data	10,263	2233	4777	2674	579	5,346	4,894	1208	1986	1459	241	447
Mean length (km)	47.7	48.2	52.0	43.8	46.6	39.5	41.5	45.1	38.8	35.7	76.1	21.3
Mean width (km)	21.1	31.4	19.7	16.8	27.1	-	-	-	-	-	-	-
Mean freeboard (m)	-	-	-	-	-	36.6	37.1	38.3	39.3	33.2	34.2	32.1

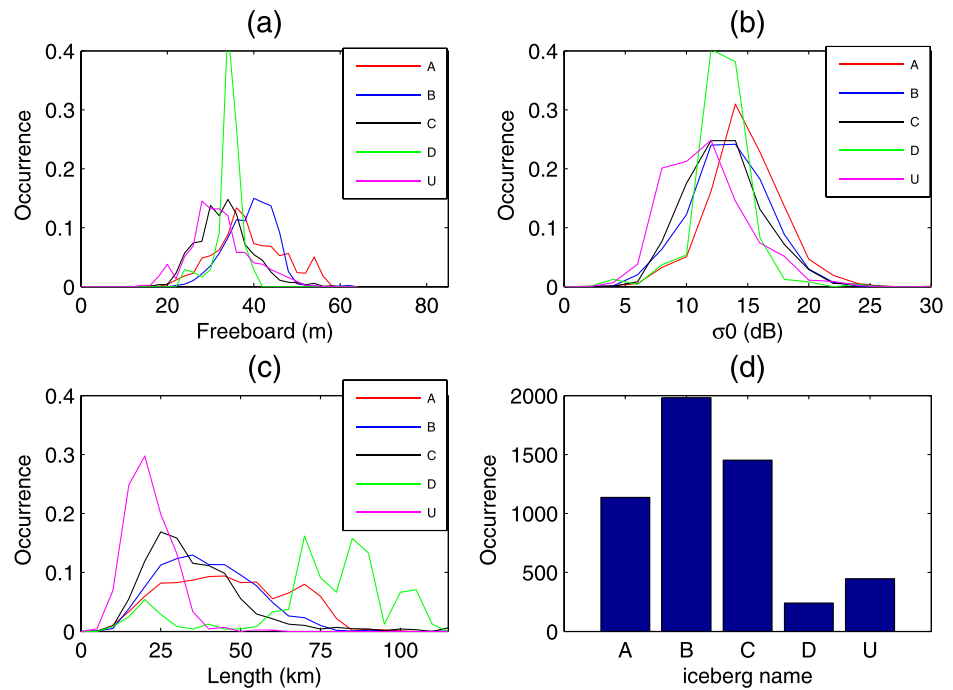


**Figure 9.** Distributions of (a) mean freeboard, (b) Mean backscatter, and (c) length as a function of the iceberg's quadrant of origin (first letter of iceberg name) and (d) number of icebergs per origin.

are associated with two large icebergs, C19a and B15j, that drifted northward and eastward within the Antarctic Circumpolar Current.

**4.2. Analysis of Individual Icebergs**

For each identified iceberg, the mean, minimum, and maximum length, the mean freeboard ( $\bar{h}$ ) and the mean backscatter ( $\bar{\sigma}_0$ ) are also estimated. The characteristics of the 207 icebergs are given in supporting

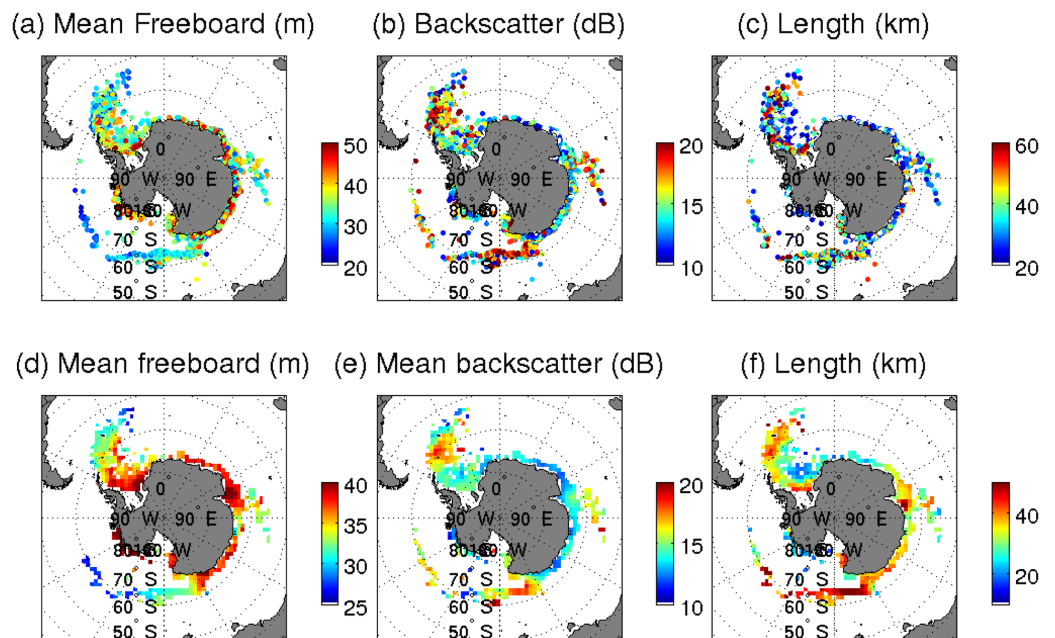


**Figure 10.** Scatter plots of the mean freeboard (a), mean backscatter (b), length (c). Mean fields on a 150 × 150 km<sup>2</sup> polar grid of mean freeboard (d), mean backscatter (e), and length (f).

**Table 3.** Statistical Analysis of Mean Size of the Individual Icebergs Using NIC and Altimeter Measurements

Database	National Ice Center					Altimeter						
Quadrant of origin	A-B-C-D	A	B	C	D	A-B-C-D-Unk	A-B-C-D	A	B	C	D	Unk
Number of icebergs	115	40	38	29	8	307	112	37	38	29	8	95
Mean length (km)	40.5	43.5	42.0	41.5	41.3	34.9	44.3	46.2	43.4	48.7	39.0	23.2
Mean width (km)	16.3	18.8	15.7	15.9	22.5	17.9	18.9	18.2	18.8	20	20.3	16.6
Min mean freeboard (m)						38.0	39.9	37.1	43.3	41.2	35.0	35.5
Max mean freeboard (m)						29.3	29.0	31.9	31.2	30.0	26.7	29.7

information Table S1. The mean values of maximum and minimum length and freeboard ( $\bar{h}$ ) are given in Table 3 as well as the corresponding values from the NIC database (for size). The distributions are presented in Figure 11. The distributions of the maximum freeboard and length present characteristics similar to the distributions of freeboard and length from the global data set while the distributions of minimum freeboard and length are narrower. The mean values of the minimum and maximum freeboard of 29.3 and 38.0 m, respectively, reflect both the natural variability of the icebergs' topography and their melting during their lifetime. The mean minimum and maximum length of 18 and 35 km results from both the randomness of the sampling by altimeters and the shapes of the icebergs. The same analysis conducted on the NIC sizes gives mean width and length of 16 and 36 km, respectively. The analysis of the distributions according to the sector of origin of the icebergs (not presented here) confirms the results of the global analysis, i.e., the highest icebergs originate in sector B and the longest ones in sector D. The analysis of the ice shelves thickness using the ice thickness data from the BEDMAP program ([http://www.antarctica.ac.uk/bas\\_research/data/access/bedmap/](http://www.antarctica.ac.uk/bas_research/data/access/bedmap/), Fretwell et al. [2013]; Lythe and Vaughan [2001]) gives a mean thickness of 317, 323, 292, and 295 m for quadrants A–D, respectively, i.e., using a height to thickness ratio of 8 a mean freeboard of 39.6, 40.3, 36.5, and 36.9 m. These values are in very good agreement with the altimeter data.

To better understand the temporal variation of the parameters, the freeboard, length, and backscatter for each iceberg has been normalized using the maximum value, defined as the median value of the five largest measurements, to avoid large outliers or potential errors, observed during the life of the iceberg.

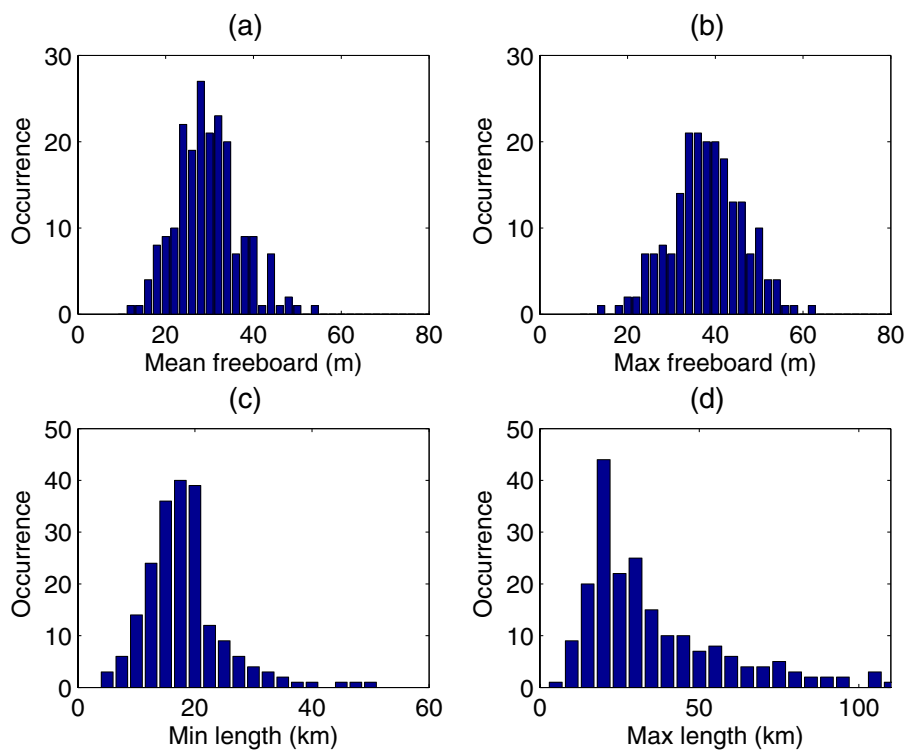


**Figure 11.** Distributions of (a) minimum freeboard, (b) maximum freeboard, (c) minimum length, and (d) maximum length of the individual icebergs.

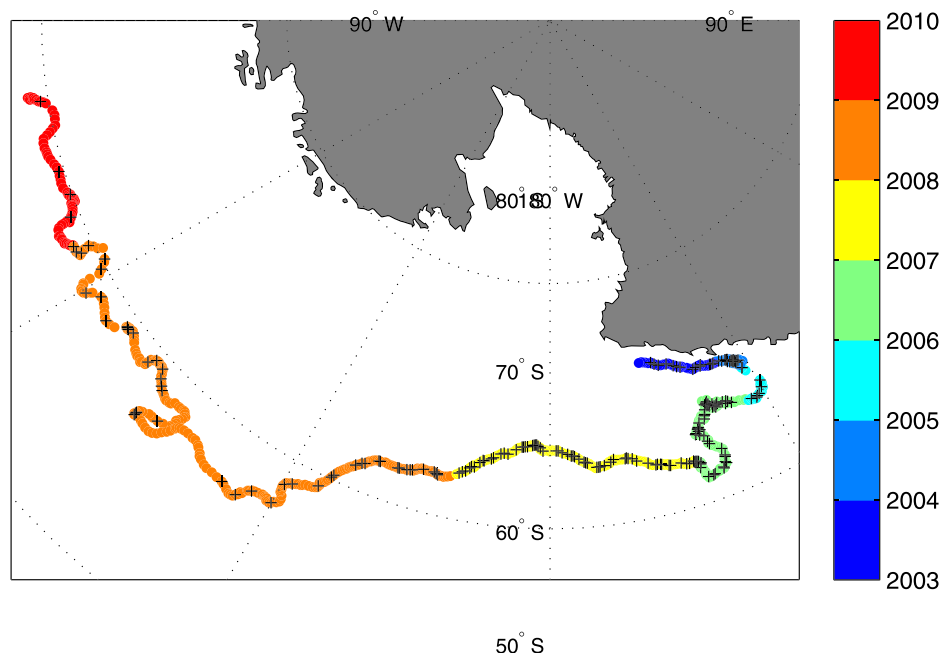


Figure 12. Track of C19a iceberg. The crosses indicate the location of the altimeter profiles.

## 5. Evolution of Icebergs

The database is used to analyze the icebergs' evolution during their lifetime. The temporal evolution of mean and maximum freeboards ( $\bar{h}$  and  $h_m$ ), mean and maximum backscatters ( $\bar{\sigma}_0$  and  $\sigma_{0m}$ ), and length of iceberg C19a during its 6 year travel from the Ross Sea to the South Pacific Ocean (see its trajectory in Figure 12) are presented in Figure 13. The sea surface temperature (SST), the SST anomaly, and the air temperature at the position of the iceberg are also shown in the figure. The daily Advanced Microwave Scanning Radiometer AMSR SST fields from Remote Sensing Systems and the ECMWF ERA Interim data have been used to estimate these parameters. Iceberg C19 is a very large iceberg that calved from the Ross Ice Shelf on May 2002. In summer 2003 C19 moved northward very rapidly, passed Cape Adare, and broke in two pieces: C19a and C19b. Between July 2003 and September 2005, C19a drifted slowly westward within sea ice along the Victoria Land coast before drifting first northward and then eastward within the Antarctic Circumpolar Current (Figure 12). Between 2003 and 2008, the NIC analysis of satellite images showed that its surface area remained constant around 5100 km<sup>2</sup> (163 km by 31 km).

During its travel in sea ice between 2003 and 2006, the C19a freeboard remained almost constant at 35 and 41 m for the mean and maximum freeboards. The freeboard standard deviation during this period was 1.9 and 2.1 m for the two estimates, respectively. These low values show that basal and surface melting and firn densification was limited while the iceberg is in sea ice in agreement with previous results from *Scambos et al.* [2005, 2008] and *Jansen et al.* [2007]. During this period, the backscatter variability was small and did not appear to correlate with surface thawing associated to positive air temperature. After February 2006, as C19a moved north in open sea characterized by positive sea SST around 1°C, it experienced strong surface melt that reflected in a strong backscatter increase of almost 10 dB and a strong decrease of freeboard elevation. The surface melt was more pronounced during the summer months during which the backscatter increased even more and could largely exceed 25 dB. This surface melt was also detected in scatterometer data during 2008 as shown by *Stuart* [2012]. Between 2006 and 2009, the freeboard regularly decreased, except in winter 2008 when it was trapped again in sea ice, while C19a traveled in open sea with SST between 0 and 4°C.

The NIC analysis showed that C19a was oblong and narrow with a width to length ratio of 5. The probability of measuring its full length is thus low. The maximum length measured by the altimeter before 2008, i.e., during the period when the iceberg's shape remained constant, is 142 km to be compared with 163 km

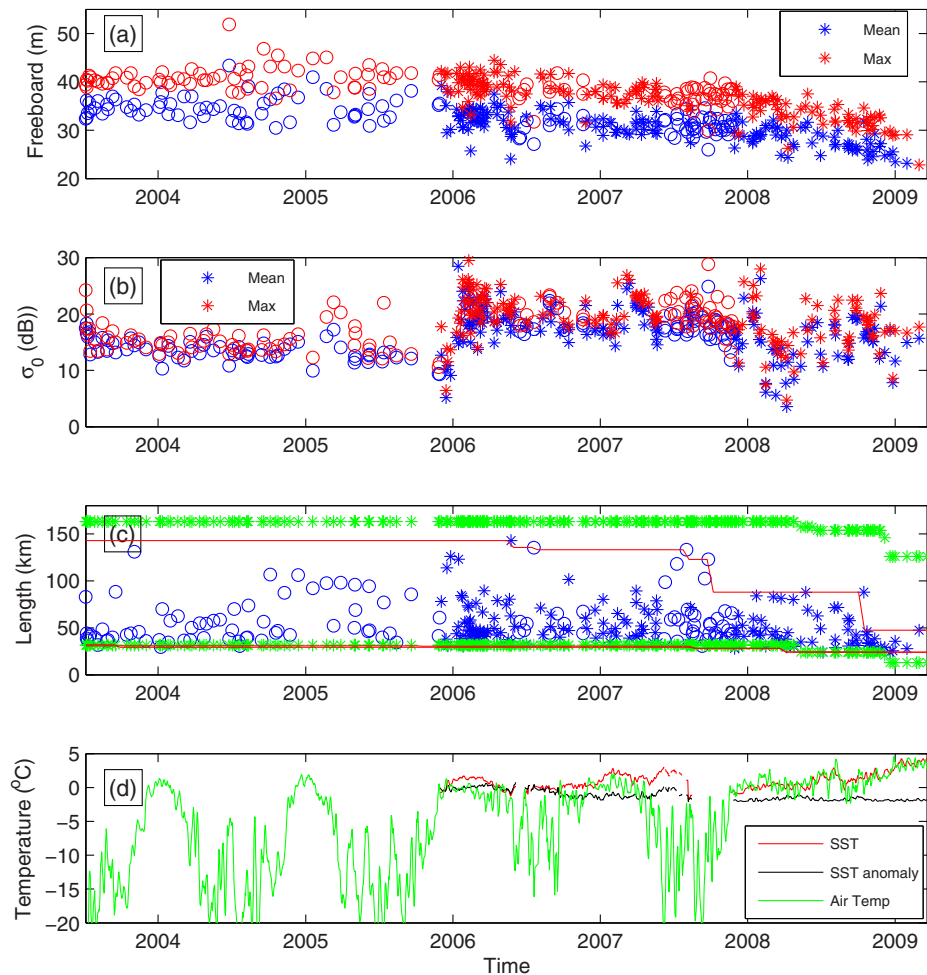


**Figure 13.** Evolution of iceberg C19a. Maximum and mean freeboard (a), maximum and mean backscatter (b), length (c), Sea Surface Temperature (red line), and SST anomaly (black line) from AMSR daily fields and air temperature from ECMWF (green line) (d). The circles and stars indicate the iceberg in sea ice and in open sea respectively. The green lines in Figure 13c represent the NIC length and width interpolated at the time of the altimeter data and the red lines the envelope of the altimeter length data.

from visible image analysis. The envelope of length data has been computed as follows: at a given time  $t$  the upper envelope is the maximum of the lengths for times greater than  $t$  and the lower envelope is the minimum of the lengths for times smaller than  $t$ . The envelope, presented in Figure 13c, gives an estimate of the temporal evolution of the length and width of the iceberg. The altimeter width is in very good agreement with the NIC one except for the very last month of C19a life. As expected the altimeter underestimates the length compared to NIC.

### 5.1. Melt Rate

To better analyze the iceberg temporal evolution, the difference between the freeboard and length and their maximum values estimated using the envelope of data has been computed. Figure 14 presents the variation of normalized freeboard (both mean and maximum) and length as a function of the cumulative number of days of positive SST. Only the data of positive SST are shown. Although the main part of the melting certainly occurs in depth of several hundreds of meters at the base of the icebergs [Jansen *et al.*, 2007; Helly *et al.*, 2011], it is, at present, impossible to get reliable in depth temperature estimates for all icebergs. As shown in Figure 13, SST can be considered as the best available proxy indicating melting. During its lifetime, the C19a freeboard decreased by almost 20 m. The change of freeboard results from the combination of basal and surface melting, firm densification, and strain thinning. Based on numerical modeling experiments of iceberg evolution (neglecting firm densification) of Jansen *et al.* [2005, 2007] estimated that

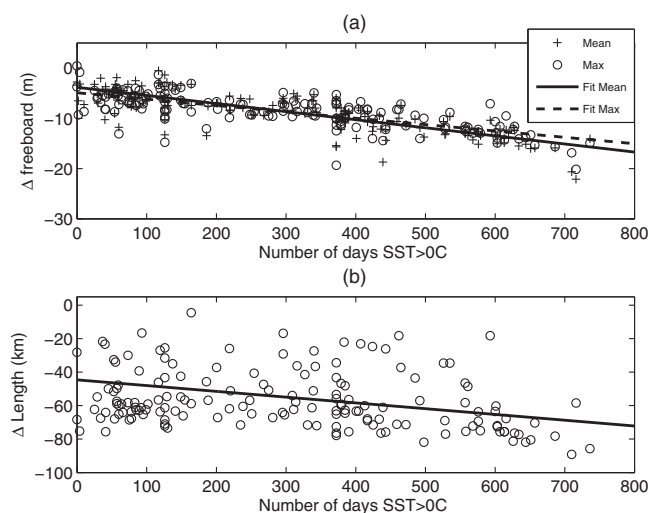


**Figure 14.** Evolution of iceberg C19a. Maximum (circles) and mean (crosses) normalized freeboard (a), normalized length (b). The lines indicate the linear regression lines of the data.

atmospheric conditions. However, the change of freeboard induced by firn densification can be estimated using a simple model. Icebergs density profile can be represented by an exponential profile in the form

$$\rho(z) = \rho_i - Ve^{Rz}$$

where  $z$  is the depth,  $\rho$  the density, and  $\rho_i$  the density of pure ice ( $915 \text{ kg}\cdot\text{m}^{-3}$ ) [West and Demarest, 1987]. The  $V$  and  $R$  model parameters are tuned so that the depths of the  $550$  and  $830 \text{ kg}\cdot\text{m}^{-3}$  densities correspond to the mean values of the firn column on big ice shelves presented by Ligtenberg et al. [2011], i.e.,  $5$  and  $45 \text{ m}$  respectively. The change of freeboard induced by firn densification is estimated by simple integration of the density profile and by assuming that the entire firn layer densifies in the same proportion. The decrease of freeboard is  $4$  and  $6.6 \text{ m}$  for a  $50\%$  and  $100\%$  densification, respectively. These values largely exceed the standard deviation of freeboard estimates and can represent a significant part of the change of freeboard. However, it is impossible to estimate reliably the firn densification and it is neglected in the study, which will lead to an overestimation of the iceberg melt rate.

The C19a change of freeboard is almost linear as a function of the number of positive SST days (see Figure 14a) and the linear regression of the data gives a rate of  $4.6 \text{ m}\cdot\text{yr}^{-1}$  for the mean freeboard and  $5.75 \text{ m}\cdot\text{yr}^{-1}$  for the maximum freeboard. Using the density profile and a mean iceberg thickness of  $320 \text{ m}$ , the mean density is  $896 \text{ kg}\cdot\text{m}^{-3}$  and thus a height to thickness ratio of  $8$ . The melt rate of C19a, neglecting the firn densification, is thus  $37$  and  $46 \text{ m}\cdot\text{yr}^{-1}$ . The normalized length shows also a clear trend of decrease with a linear trend of  $3.5 \text{ m}\cdot\text{d}^{-1}$ . However, because of the particular sampling by altimeters, the result has to be considered with caution.

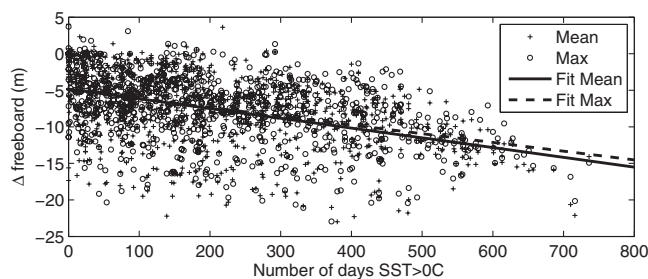


**Figure 15.** Melting icebergs; Maximum (circles) and mean (crosses) normalized freeboards for icebergs in open sea. The lines indicate the linear regression lines of the data.

95% of the decrease of thickness was caused by basal melting, 1% by surface melting and 4% by strain thinning. Surface melting and strain thinning are thus neglected in our study.

After calving, the icebergs density profile is similar to that of the parent ice shelf. During their lifetime, surface melting and weathering can compact the icebergs top snow/firn layer with no change of mass resulting in a decrease of freeboard. The process of firn densification is complex and although several models have been developed for ice sheet [Arthern et al., 2010; Li and Zwally, 2011; Ligtenberg et al., 2011], at present, no reliable model exists for icebergs that experienced more variable oceanic and

The melt rate of icebergs has also been estimated using all the individual icebergs that travel in open sea with positive SST during the 2002–2012 period. Figure 15 presents the 933 normalized freeboards ( $\bar{h}$  and  $h_m$ ) as a function of the cumulative number of positive SST. Only the data with positive SST are considered. The linear regression of the data gives a rate of  $4.3 \text{ m}\cdot\text{yr}^{-1}$  and  $4.8 \text{ m}\cdot\text{yr}^{-1}$  for the mean and maximum freeboards, respectively, i.e., melt rates of  $35$  and

$39 \text{ m}\cdot\text{yr}^{-1}$ . The mean SST for all data is  $1.1^\circ\text{C}$ . These values are of the same order of magnitude as the melt rate presented by *Neshyba and Josberger* [1980] for a thermal driving of  $2^\circ\text{C}$  or the values ( $4 \text{ m}\cdot\text{month}^{-1}$ ) presented by *Jansen et al.* [2007] for iceberg A38b using a physical model calibrated by ICESat profiles.

## 5.2. Volume of Ice

### 5.2.1. Estimation of the Total Volume of Ice

The NIC/BYU and altimeter database are combined to produce a new database containing the daily location, size, and freeboard elevation of all icebergs. The daily location of each iceberg is estimated from the BYU locations. For most icebergs, BYU provides a daily position. For the few missing days, the location is obtained by simple linear interpolation. The iceberg's size is obtained by linear interpolation in time of the NIC length and width when available, or else of the altimeter maximum and minimum length envelope. The large variations of size result from iceberg breaking and are thus sporadic events. Because of the large time lag that can exist between two NIC estimates of size, it is impossible to determine their exact time of occurrence. The temporal linear interpolation smoothes the potential bias over the time lag between two size estimates. The freeboard is the time interpolated altimeter estimate of the mean freeboard  $\bar{h}$ . For the three NIC icebergs never sampled by the altimeters, the freeboard is fixed to the mean freeboard of their quadrant of origin.

At any given day, there are 50–80 icebergs with size and freeboard data and 10–30 icebergs with no data (see Figure 16b). These icebergs with no data are 95% of the time of the “UK” category, i.e., icebergs smaller than 10–15 nm. Assuming that the iceberg's surface follows the lognormal distribution of NIC icebergs ( $\mu=5.8$  and  $\sigma^2=1.95$ , i.e., mean of  $857 \text{ km}^2$ ), the icebergs whose area is smaller than  $400 \text{ km}^2$  represent about 50% of the population but only 19% of the total surface. Icebergs smaller than  $200 \text{ km}^2$  constitute 39% of the ensemble but contribute less than 8% to the total surface. The unknown icebergs do not account for a large volume of ice. The 30–40 icebergs larger than  $400 \text{ km}^2$  represent thus most of the surface and volume of ice ( $\sim 80\%$ ). It should be noted that this argument is valid for icebergs larger than 6 km; if all icebergs size were considered the proportion of the total volume contained by the largest icebergs would be smaller. For example, if we assume a lognormal distribution of  $0.01 \text{ km}^2$  mean and a  $\sigma^2=1.95$ , the proportion of volume for icebergs larger than  $400 \text{ km}^2$  is only 62%.

The merged database enables a first-order approximation estimation of the daily volume of ice in the Southern Ocean using the constant height to thickness ratio of 8 presented in section 5.1. The comparison of the total daily volume of ice estimated using only the NIC size estimates and the one using only the altimeter ones confirms that the altimeters underestimate the surface of the icebergs especially for very large icebergs (see Figure 16a) because they do not always sample their longer length. This is particularly noticeable from 2002 to 2006 when the two largest icebergs ever recorded, B15 and C19, are present. The addition of altimeter data, that concerns mainly the unknown category of icebergs, modifies only marginally (by 2–3%) the total volume of ice. Between 2002 and 2012, the daily volume of ice steadily decreases from  $2.2 \times 10^4 \text{ km}^3$  to  $0.9 \times 10^4 \text{ km}^3$  while the number of icebergs larger than  $400 \text{ km}^2$  decreases from 35 to 21. The linear regression of volume gives a mean decrease of  $1200 \text{ km}^3$  per year between 2002 and 2012.

The uncertainties on volume estimates are quite difficult to quantify because of the scarcity of validation data. However, the freeboard uncertainty can be estimated by computing the standard deviations of freeboard measurements of individual icebergs for which the cumulative time of positive temperature is nil, i.e., when icebergs are most probably not melting. The mean freeboard std is  $3 \pm 1.5 \text{ m}$  or  $8 \pm 4\%$ . This small std value for the ensemble of icebergs confirms that basal melting and firn compaction are limited when icebergs are within sea ice and that they can be neglected in a first-order approximation. The errors due to firn compaction and to uncertainties on the freeboard to thickness ratio can be of the order of several meters (about 4 m for a 50% densification) as shown in section 5.1. The thickness uncertainty should thus be of the order of 10–20%. The uncertainty on the size estimate should be of the order of 10% resulting in an uncertainty of the order of 20–30% on the volume estimate.

In 2002, the total volume of ice represents 14–15 times the total annual calving flux estimated at  $1321 \pm 44 \text{ Gt}$  (i.e.,  $1500 \text{ km}^3$  assuming a mean iceberg density of  $892 \text{ kg}\cdot\text{m}^{-3}$ ) by *Depoorter et al.* [2013] who combined ice thickness measurements from altimetry and ground radar and surface velocity from SAR interferometry to calculate the mean flux for the 1979–2010 period. In 2012, the total volume reduces to about 6–7

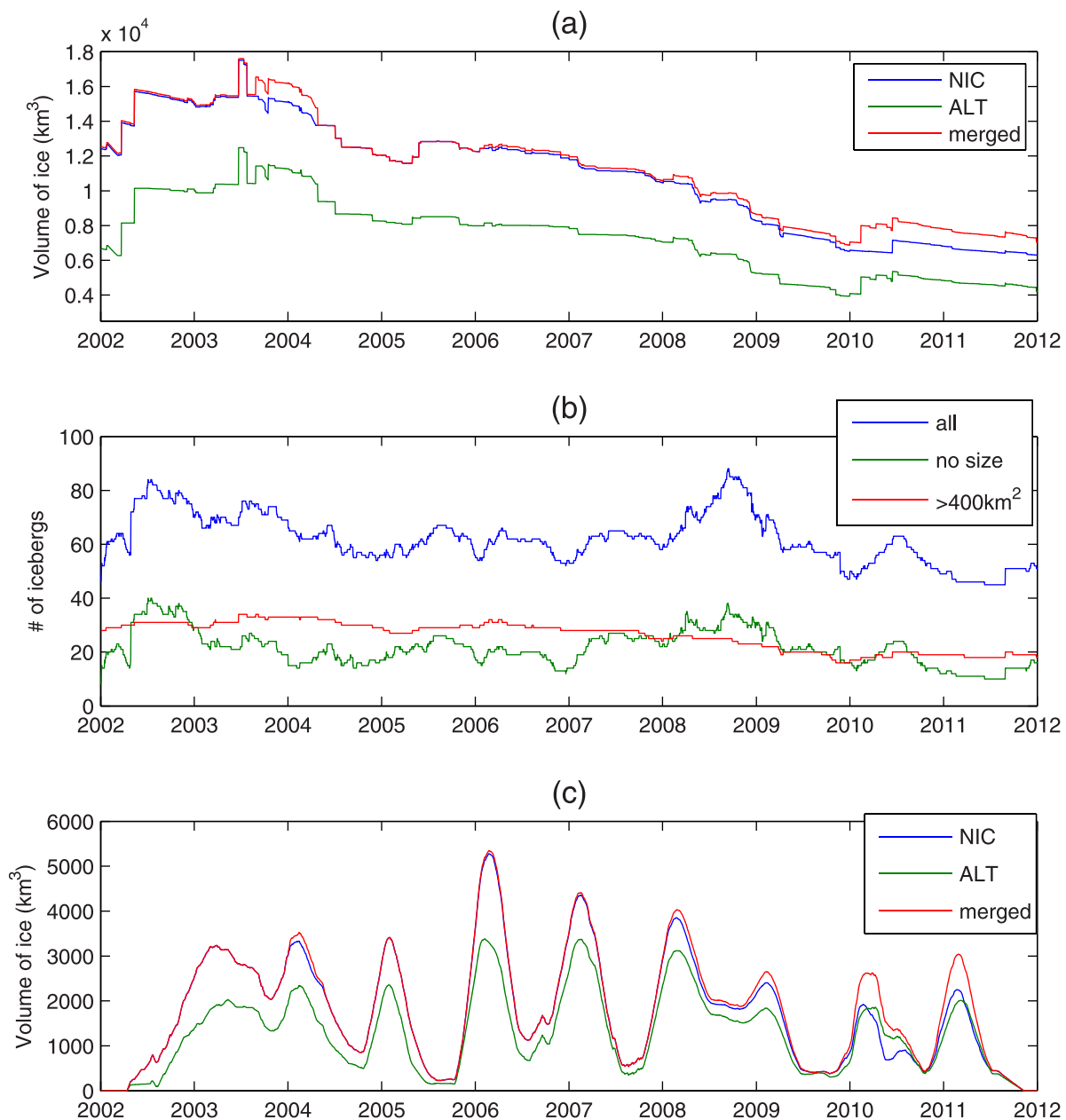


**Figure 16.** Total daily volume of ice from the NIC database (blue line), the altimeter database (green line), and the merged database (red line) (a). Number of icebergs (blue line), of icebergs with no size data (green line), and of icebergs larger than 400 km<sup>2</sup> (red line) (b). Volume of ice in open sea from the NIC database (blue line), the altimeter database (green line), and the merged database (red line) (c).

years of calving. The very large amount of ice present in 2002 could result from the large increase in the number of large icebergs reported by *Long et al.* [2002] for the 1997–2000 period and the calving of the two largest icebergs ever recorded, B15 in 2000 and C19 in 2002 representing they alone more than 6000 km<sup>3</sup>. From 2002 to 2012, the volume of ice steadily decreases with an exception in 2005 due to the calving of D15 iceberg. This volume variability could reflect the decadal variability of giant icebergs calving reported by *Jacobs et al.* [1992].

The volume of ice that can significantly melt and contributes to the freshwater flux in the ocean can be estimated by considering only the icebergs present in the open ocean, characterized by positive SSTs. This volume presents a strong seasonal cycle reflecting the variation of sea ice extent. During summer, the volume is of the order of  $4 \times 10^3$  km<sup>3</sup> and can reach  $7 \times 10^3$  km<sup>3</sup> in summer of 2006 (see Figure 16c). The volume

of ice in open ocean represents between half (in 2006) and one fifth (in 2003) of the total volume of ice. In winter, many icebergs are trapped in sea ice and the volume in open sea strongly decreases. However, during some winters like 2003, 2004, 2006, or 2008, the volume of ice in open sea is still significant and can reach or exceed  $2 \times 10^3 \text{ km}^3$  as in 2008 when C19a traveled in the South Pacific north of  $55^\circ\text{S}$ .

The geographical mean distribution of the volume of ice for the period 2002–2012 is presented in Figure 17. The ice concentrates mainly within the Antarctic coastal current and along the Antarctic Peninsula and in the “iceberg alley” of the South Atlantic ocean. A small regional maximum associated with the Pine Island glacier ( $100^\circ\text{W}$ ,  $75^\circ\text{S}$ ) is clearly visible in the Amundsen Sea. The mean volume of ice is of the order of  $100 \text{ km}^3$  per grid cell of  $150 \times 150 \text{ km}^2$  along the Antarctic Peninsula and Eastern Antarctica. It is of the order of  $10 \text{ km}^3$  in the South Atlantic Ocean. During the period considered, the South Pacific and Indian oceans north of  $65^\circ\text{S}$  are characterized by sporadic occurrences of large icebergs that can travel for several years over very long distances and can locally give very high content of ice that can impact the ocean circulation.

### 5.2.2. Analysis of the Volume Variations

The variations of the volume of ice result from three main causes: (i) input of new icebergs calving from emissary glaciers and ice shelves, (ii) basal melting, and (iii) breaking into pieces too small to be detected by NIC. To determine (i) and (iii), it is necessary to know the origin and destiny of each iceberg. The genealogical tree of all the icebergs has been created to determine if an iceberg has parents and sons. Supporting information Figures S1–S3 present the timetable and genealogical trees of all icebergs. For example, C19 is the parent of C19a and C19b. The input of ice (i) is simply the volume of icebergs with no parents, i.e., that calve from ice sheet or glaciers. The basal melting (ii) is estimated as the sum of the products of iceberg surface,  $S_i$ , and the daily variation of thickness,  $dT_i$

$$M = \sum_{i=1}^N S_i dT_i \tag{1}$$

The breaking,  $B$ , (iii) is the sum of the volume of icebergs with no sons,  $B_{ns}$  and of small pieces that calve from the large ones. The second term,  $B_s$  is estimated by the sum of the products of thickness,  $T$ , by the daily variation of surface,  $dS$

$$B_s = \sum_{i=1}^N dS_i T_i \tag{2}$$

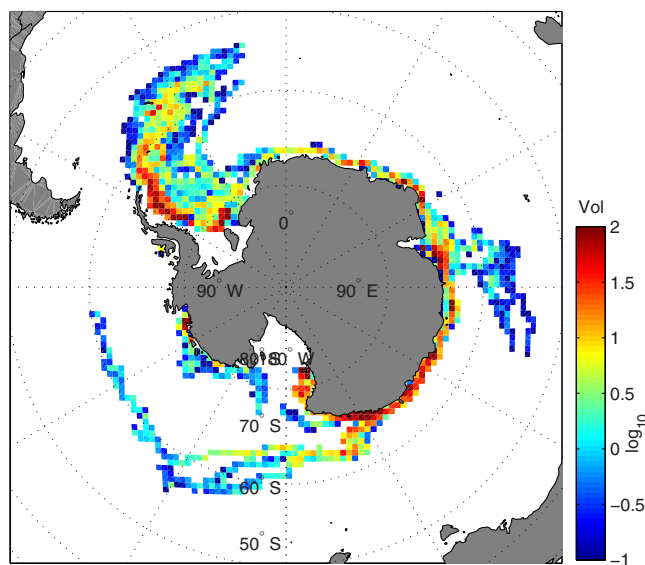


**Figure 17.** Mean daily volume of ice on a  $150 \times 150 \text{ km}^2$  regular polar grid for the 2002–2012 period estimated from the merged iceberg database. The color scale is logarithmic.

Figure 18 presents the cumulative sums of the input of ice, the total volume loss ( $M + B$ ), the basal melting ( $M$ ), and the breaking of icebergs ( $B$ ). During the 11 year period the input of ice is quite linear. To take into account the errors on icebergs volume estimates, the rate of change and its uncertainties are estimated using a bootstrap method. A 30% Gaussian random noise corresponding to the estimated volume error is added before computing the cumulative sum. The linear fit as a function of time is calculated and the process is iterated 10,000 times. The mean and std of the rate of change of the estimates are then computed. The input of ice is about  $960 \pm 72 \text{ km}^3 \cdot \text{yr}^{-1}$ . This input corresponds to the proportion

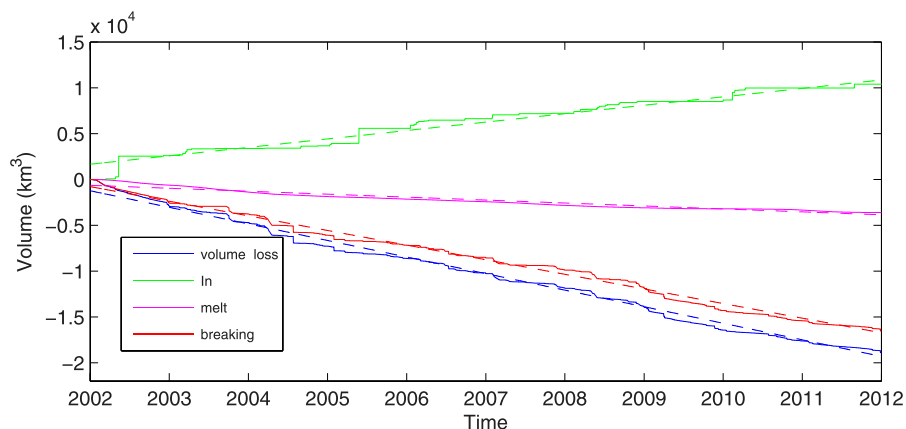


**Figure 18.** Variation of the volume of ice. Cumulative total loss of volume (blue line), input of ice (green line), volume loss by melting (magenta line), and volume loss by breaking (red line). The dashed lines represent the linear regression of the data.

of the total calving flux of the Antarctic ice shelves due to icebergs larger than 6 km in length. It represents about 60% of the total calving flux of  $1331 \pm 44 \text{ Gt}\cdot\text{yr}^{-1}$  ( $\sim 1500 \text{ km}^3$ ) estimated by *Depoorter et al.* [2013] for the 1979–2012 period. The difference can result from smaller icebergs calving from the ice sheet and/or from a decrease of calving at a decadal time scale.

During the 2002–2012 period, the strong decrease of the total volume results from a total loss of ice twice as large as the input ( $\sim 1800 \pm 40 \text{ km}^3\cdot\text{yr}^{-1}$ ). This clearly shows that the system is out of equilibrium. After a very large input of ice in the late 1990s and early 2000s, the system slowly returns to a state where the loss and input of ice would be in equilibrium. During this period, the large loss of ice corresponds to a strong increase of freshwater flux into the ocean that can potentially modify the Southern Ocean circulation.

Basal melting contributes to about 18% of the total loss ( $320 \pm 5 \text{ km}^3\cdot\text{yr}^{-1}$ ) while breaking represents 82% at  $1,500 \pm 40 \text{ km}^3\cdot\text{yr}^{-1}$ . One third ( $430 \pm 15 \text{ km}^3\cdot\text{yr}^{-1}$ ) of breaking takes place in open water, i.e., characterized by positive SST. This value is close to the mean value of the total volume of ice for icebergs smaller than 3 km ( $\sim 400\text{--}500 \text{ km}^3\cdot\text{yr}^{-1}$ ) detected by altimeter [*Tournadre et al.*, 2012].

### 5.3. Estimation of Iceberg Backscatter

The altimeter database also provides an opportunity for analysis of the Ku band backscatter of the ice constituting icebergs. This backscatter estimate is crucial to calibrate and validate the models used to infer the

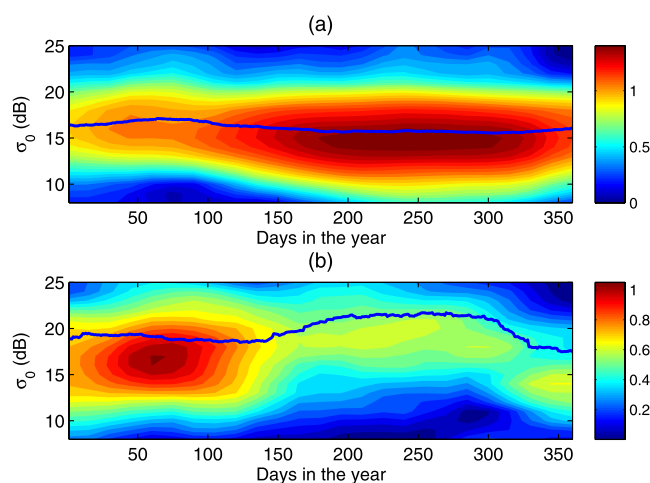


**Figure 19.** Bidimensional histogram of backscatter and Julian day in the year for (a) icebergs in sea ice (b) icebergs in open sea. The blue lines represent the mean backscatter as a function of Julian day.

area of small icebergs from the analysis of altimeter waveform data, which assumes a constant backscatter of ice of 19 dB at Ku band for icebergs in open sea [*Tournadre et al.*, 2012]. Figure 19 presents the bidimensional histogram of backscatter and Julian day in the year for icebergs in sea ice and in open sea. For icebergs trapped in sea ice, the mean backscatter is about 16 dB and presents a small seasonal variability ( $\sim 1 \text{ dB}$ ) with a maximum in February and a minimum in August. During winter, the variability of backscatter increases related to the presence of snow. For icebergs traveling in open sea, the mean backscatter is about 20 dB. The apparent seasonal cycle

( $\sim 3$  dB) with a maximum in summer (March–April) and a minimum in winter (August) results mainly from the fact that the icebergs present in open sea in winter are located much further north in certainly warmer seas and have certainly melted for a longer time than those present in summer.

## 6. Conclusions

Because of the scarcity of information on the icebergs freeboard and thickness, there are still large uncertainties on the volume of ice transported by the large Antarctica icebergs and thus on the freshwater flux in the Southern Ocean, key parameters for climate studies. The combined use of the large icebergs data base from NIC and BYU and of altimeters (Jason-1, Jason-2, and Envisat) archives allows the creation of a database containing 5366 icebergs freeboards elevation profiles, lengths, and backscatter profiles covering the 2002–2012 period. All the icebergs detected by NIC during the period but three and about 50% of the smaller ones ( $< 16$  km) detected by BYU are sampled at least once by altimeter. The mean time between two samplings is 32 days for the NIC icebergs and 42 for the BYU ones.

Freeboard measurements have been validated by comparison of altimeter profiles over iceberg A38b with maps of freeboard computed using an initial shape estimated from Ice shelf elevation data and a melting model calibrated using the ICESat profiles from *Jansen et al.* [2007]. The difference between the ICESat and altimeter elevation is better than 1.5 m.

The analysis of the database shows that the distributions of maximum and mean freeboards, length, and backscatter show significant differences as a function of the icebergs' quadrant of origin (A— $0^\circ$ – $90^\circ$ W; B— $90^\circ$ W– $180^\circ$ ; C— $90^\circ$ E– $180^\circ$ ; D— $0^\circ$ – $90^\circ$ E). The highest icebergs originate from sector B (39.3 m mean freeboard) while the lowest from sector C (33.2 m). The longest come from quadrant A (45.1 km mean length) and the shortest from sector C (35.7 km). The overall icebergs length follows well a lognormal distribution of 39.5 km mean. The icebergs detected only by BYU using scatterometer data are, as expected, significantly smaller with a mean length of 21 km but also significantly lower with a mean freeboard of 32 m. The mean characteristics of icebergs as a function of their quadrant of origin could be used as input for ocean circulation model including icebergs.

The temporal variability of length and width of icebergs is estimated by computing the envelope of all the altimeter length and freeboard measurements. The normalized freeboard and length of each iceberg are estimated by difference to their maximum values. Neglecting surface melting, strain thinning, and firn densification, the melt rate, computed by linear regression of the normalized freeboards, and the cumulative number of positive SST's days, is about  $40 \text{ m}\cdot\text{yr}^{-1}$  for a mean SST around  $1^\circ\text{C}$ . This value is in the same range of values as previous melt rate published by *Neshyba and Josberger* [1980] and *Jansen et al.* [2007].

Combining the altimeter and NIC/BYU databases a daily iceberg database of location, size, and freeboard elevation has been created. Between 50 and 95 icebergs are always present around Antarctica, among which 10 to 30 are not sampled by altimeters. The icebergs not sampled are 95% of the time smaller icebergs only detected by BYU and they should not represent a significant amount of ice. The iceberg volume is estimated using the altimeter freeboards and the NIC sizes when available or the altimeter ones if not. The total ice volume represented in 2002 14–15 times the total annual calving flux estimated at  $1321 \pm 44\text{Gt}$  ( $\sim 1500 \text{ km}^3$ ) by *Depoorter et al.* [2013], and decreased regularly to about 6–7 years of calving in 2012. The very large amount of ice of 2002 could result from the large increase of the number of large icebergs reported by *Long et al.* [2002] for the 1997–2000 period and the calving of the two largest icebergs ever recorded (B15 and C19) in 2000 and 2002. It could also reflect the decadal variability of giant icebergs calving reported by *Jacobs et al.* [1992].

The ice volume variation depends on three main causes: (i) input of new icebergs, (ii) basal melting, and (iii) breaking into pieces too small to be detected by NIC and BYU. During the 2002–2012 period, the mean input of ice by calving of icebergs larger than 6 km is  $960 \pm 72 \text{ km}^3\cdot\text{yr}^{-1}$  i.e., about 60% of the total calving flux of *Depoorter et al.* [2013]. The mean total loss of ice is twice as large as the input at  $1,800 \pm 40 \text{ km}^3\cdot\text{yr}^{-1}$ . Calving of large icebergs is in large part a stochastic process, the input of ice is therefore sporadic and large quantities of ice can feed the system in a very short time. Melting and breaking are more regular processes with much longer time scales than calving. Thus, after the very large input of ice in the late 1990s and early 2000s, the system returns slowly to a more balanced state where the loss and input of ice are almost in equilibrium.

Eventually, this condition might again be broken by some new very large inputs of ice. During the return to equilibrium phase, the loss of ice would certainly result in an increase of the freshwater flux into the Southern Ocean through breaking into smaller icebergs and melting. This larger amount of freshwater could inhibit the ventilation of deep waters around Antarctica, causing a warming of the deep ocean, and a cooling of the surface [Richardson *et al.*, 2005]. It could also favor an increase in sea ice extent and thickness by cooling and freshening the upper water layer [Jongma *et al.*, 2009].

Basal melting represents about one fifth of the total loss of ice while breaking into smaller icebergs not detected by NIC and BYU represents 80% of the total loss. These results show that although large icebergs carry most of the volume of ice they contribute only marginally to the freshwater flux that would mainly result from the melting of smaller icebergs that will act as a diffusive process and will transport large amount of ice far away from the large icebergs as already shown by Tournadre *et al.* [2012].

Finally the database has also been used to estimate the mean backscatter of iceberg in open sea, a crucial parameter for the detection of smaller icebergs (<2–3 km) using altimeter data [Tournadre *et al.*, 2012]. For icebergs in open sea, the mean backscatter is about 20 dB at Ku band.

#### Acknowledgments

The authors are greatly indebted to Chris Readinger from the National Ice Center who kindly provided a copy of the southern icebergs database. AMSR data are produced by Remote Sensing Systems and sponsored by the NASA Earth Science MEaSUREs DISCOVER Project and the NASA AMSR-E Science Team. Data are available at [www.remss.com](http://www.remss.com). The altimeter data (Sensor Geophysical Data Records) were provided by AVISO for Jason-1 and Jason-2 and by the European Space Agency for Envisat. The study was partially founded by the French Centre National d'Etudes Spatiales through the TOSCA program.

#### References

- Arthern, R., D. Vaughan, A. Rankin, R. Mulvaney, and E. R. Thomas (2010), In situ measurements of Antarctic snow compaction compared with predictions of models, *J. Geophys. Res.*, *115*, F03011, doi:10.1029/2009JF001306.
- Benn, D., C. Warren, and R. Mottram (2007), Calving processes and the dynamics of calving glaciers, *Earth Sci. Rev.*, *82*, 143–179.
- Brown, G. S. (1977), The average impulse response of a rough surface and its applications, *IEEE Trans. Antennas Propag.*, *AP-25*, 67–74.
- Chelton, D. E., J. C. Ries, B. J. Haines, L.-L. Fu, and P. S. c. Callahan (2001a), Chap. 1: An introduction to satellite altimetry, in *Satellite Altimetry 589 and Earth Science: A Handbook of Techniques and Applications*, vol. 463, pp. 1–122, edited by L. Fu and A. Cazenave, Academic Press, San Diego, Calif.
- Depoorter, M. A., J. L. Bamber, J. A. Griggs, J. T. M. Lenaerts, S. R. M. Ligtenberg, M. R. van den Broeke, and G. Moholdt (2013), Calving fluxes and basal melt rates of Antarctic ice shelves, *Nature*, *502*, pp. 89–92, doi:10.1038/nature12567.
- Fretwell, P., et al. (2013), Bedmap2: Improved ice bed, surface and thickness datasets for Antarctica, *Cryosphere*, *7*(1), 375–393, doi:10.5194/tc-7-375-2013.
- Gladstone, R. M., G. R. Bigg, and K. W. Nicholls (2001), Iceberg trajectory modeling and meltwater injection in the Southern Ocean, *J. Geophys. Res.*, *106*, 19,903–19,916, doi:10.1029/2000JC000347.
- Gommenginger, C., P. Thibaut, L. Fenoglio-Marc, G. Quartly, X. Deng, J. Gomez-Enri, P. Challenor, and Y. Gao (2011), Retracking altimeter waveforms near the coasts, in *Coastal Altimetry*, edited by S. Vignudelli et al., pp. 61–101, Springer, Berlin, doi:10.1007/978-3-642-12796-04.
- Helly, J. J., R. S. Kaufmann, G. R. Stephenson Jr., and M. Vernet (2011), Cooling, dilution and mixing of ocean water by free-drifting icebergs in the Weddell Sea, *Deep Sea Res., Part II*, *58*(11–12), 1346–1363, doi:10.1016/j.dsr2.2010.11.010.
- Jacobs, S. S., H. Hellmer, C. S. M. Doake, A. Jenkins, and R. Frolich (1992), Melting of ice shelves and the mass balance of Antarctica, *J. Glaciol.*, *38*(130), 375–387.
- Jansen, D., H. Sandhager, and W. Rack (2005), Evolution of tabular iceberg A-38B, observation and simulation, in *Proceedings of the 18th Forum Research into Ice Shelf Processes, FRISP Rep. 16*, edited by L. Smedsrud, pp. 13–17, Alfred Wegener Inst., Helgoland, Germany.
- Jansen, D., M. Schodlok, and W. Rack (2007), Basal melting of A-38B: A physical model constrained by satellite observations, *Remote Sens. Environ.*, *111*(2–3), 195–203, doi:10.1016/j.rse.2007.03.022.
- Jongma, J. I., E. Driesschaert, T. Fichet, H. Goosse, and H. Renssen (2009), The effect of dynamic-thermodynamic icebergs on the Southern Ocean climate in a three-dimensional model, *Ocean Modell.*, *26*(1–2), 104–113, doi:10.1016/j.ocemod.2008.09.007.
- Lambin, J., et al. (2010), The OSTM/Jason-2 Mission, *Mar. Geod.*, *33*, 4–25, doi:10.1080/01490419.2010.491030.
- Lancelot, C., A. de Montety, H. Goosse, S. Becquevort, V. Schoemann, B. Pasquer, and M. Vancoppenolle (2009), Spatial distribution of the iron supply to phytoplankton in the Southern Ocean: A model study, *Biogeosciences*, *6*, 2861–2878.
- Legrésy, B. (1995), Etude du retracking des formes d'ondes altimétriques au-dessus des calottes polaires, *Tech. Rep.*, CNES report CT/ED/TU/UD/96.188, CNES contract 856/2/95/CNES/0060, CNES, Toulouse, France.
- Li, J., and H. Zwally (2011), Modeling of firn compaction for estimating ice-sheet mass change from observed ice-sheet elevation change, *Ann. Glaciol.*, *52*(59), 1–7.
- Ligtenberg, S. R. M., M. M. Helsen, and M. R. van den Broeke (2011), An improved semi-empirical model for the densification of Antarctic firn, *Cryosphere*, *5*(4), 809–819, doi:10.5194/tc-5-809-2011.
- Long, D., J. Ballantyne, and C. Bertoina (2002), Is the Number of Icebergs Really Increasing?, *EOS Trans. AGU*, *83*(42), 469–474, doi:10.1029/2002EO000330.
- Lythe, M. B., and D. G. Vaughan (2001), BEDMAP: A new ice thickness and subglacial topographic model of Antarctica, *J. Geophys. Res.*, *106*, 11,335–11,351, doi:10.1029/2000JB900449.
- Martin, T., and A. Adcroft (2010), Parameterizing the fresh-water flux from land ice to ocean with interactive icebergs in a coupled climate model, *Ocean Modell.*, *34*(3–4), 111–124, doi:10.1016/j.ocemod.2010.05.001.
- McIntyre, N. F., and W. Cudlip (1987), Observation of a giant Antarctic tabular iceberg by satellite radar altimetry, *Polar Rec.*, *145*, 458–462.
- Ménard, Y., and L. Fu (2001), Jason-1 mission, in *Aviso Newsletter*, vol. 8, AVISO Altimetry Edition, Toulouse, France.
- Neshyba, S., and E. G. Josberger (1980), On the estimation of Antarctic iceberg melt rate, *J. Phys. Oceanogr.*, *10*, 1681–1685.
- Queffeuilou, P. (2013), Merged altimeter wave height data base: An update, in *Proceedings of ESA Living Planet Symposium*, vol. SP-722, European Space Agency, Noordwijk, Netherlands.
- Raiswell, R., L. G. Benning, M. Tranter, and S. Tulaczyk (2008), Bioavailable iron in the Southern Ocean: the significance of the iceberg conveyor belt, *Geochem. Trans.*, *9*, doi:10.1186/1467-4866-9-7.

- Resti, A., J. Benveniste, M. Roca, and G. Levrini (1999), The Envisat Radar Altimeter System (RA-2), in *ESA Bull.* 98, edited by J. Johannessen, ESA Directorate for Applications Programmes, ESTEC, Noordwijk, Netherlands.
- Richardson, G., M. R. Wadley, K. J. Heywood, D. P. Stevens, and H. T. Banks (2005), Short-term climate response to a freshwater pulse in the Southern Ocean, *Geophys. Res. Lett.*, 32, L03702, doi:10.1029/2004GL021586.
- Rignot, E., S. Jacobs, J. Mouginot, and B. Scheuchl (2013), Ice-shelf melting around Antarctica, *Science*, 341, 266–270.
- Scambos, T., O. Sergienko, A. Sargent, D. McAyeal, and J. Fastbook (2005), ICESat profiles of tabular iceberg margins and iceberg breakup at low latitudes, *Geophys. Res. Lett.*, 32, L23509, doi:10.1029/2005GL023802.
- Scambos, T., R. Ross, R. Bauer, Y. Yermolin, P. Skvarca, D. Long, J. Bohlander, and T. Haran (2008), Calving and ice-shelf break-up processes investigated by proxy: Antarctic tabular iceberg evolution during northward drift, *J. Glaciol.*, 54(187), 579–591, doi:10.3189/002214308786570836.
- Schodlok, M. P., H. H. Hellmer, G. Rohardt, and E. Fahrbach (2006), Weddell sea iceberg drift: Five years of observations, *J. Geophys. Res.*, 111, C06018, doi:10.1029/2004JC002661.
- Schwarz, J. N., and M. P. Schodlok (2009), Impact of drifting icebergs on surface phytoplankton biomass in the Southern Ocean: Ocean colour remote sensing and in situ iceberg tracking, *Deep Sea Res., Part I*, 56(10), 1727–1741, doi:10.1016/j.dsr.2009.05.003.
- Silva, T., G. Bigg, and K. Nicholls (2006), The contribution of giant icebergs to the Southern Ocean freshwater flux, *J. Geophys. Res.*, 111, C03004, doi:10.1029/2004JC002843.
- Smith, K. L. (2011), Free-drifting icebergs in the Southern Ocean: An overview, *Deep Sea Res., Part II*, 58(11–12), 1277–1284, doi:10.1016/j.dsr2.2010.11.003.
- Stuart, K. (2012), Application of seawinds scatterometer data to the study of Antarctic icebergs, PhD thesis, Brigham Young Univ., Microwave Earth Remote Sensing Lab., Provo, Utah.
- Stuart, K. M., and D. G. Long (2011), Tracking large tabular icebergs using the SeaWinds Ku-band microwave scatterometer, *Deep Sea Res., Part II*, 58(11–12), 1285–1300, doi:10.1016/j.dsr2.2010.11.004.
- Tournadre, J., B. Chapron, and N. Reul (2011), High-resolution imaging of the ocean surface backscatter by inversion of altimeter waveforms, *J. Atmos. Oceanic Technol.*, 28, 1050–1062, doi:10.1175/2011JTECHO820.1.
- Tournadre, J., F. Girard-Ardhuin, and B. Legresy (2012), Antarctic icebergs distributions, 2002–2010, *J. Geophys. Res.*, 117, C05004, doi:10.1029/2011JC007441.
- West, J. C., and R. Demarest (1987), The radiation characteristics of an arbitrary antenna positioned on a polar ice sheet, *Geophysics*, 52, 1689–1696.